

Ion irradiation of novel yttrium/ytterbium-based pyrochlores: The effect of disorder

Karl R. Whittle^{a,*}, Mark G. Blackford^a, Robert D. Aughterson^a, Gregory R. Lumpkin^a,
Nestor J. Zaluzec^b

^a Institute of Materials Engineering, ANSTO, PMB 1, Menai, NSW 2234, Australia

^b Materials Science Division, Argonne National Laboratory, 9700 South Cass Avenue, IL 60439, USA

Received 21 July 2011; received in revised form 9 September 2011; accepted 11 September 2011

Available online 15 October 2011

Abstract

Pyrochlores based on the general composition Ln_2TiO_5 ($\text{Ln}_{2.67}\text{Ti}_{1.33}\text{O}_{6.67}$) and $\text{Ln}_2\text{Ti}_2\text{O}_7$, where $\text{Ln} = \text{Y}$ or Yb , have been irradiated through the crystalline–amorphous transition with 1 MeV Kr ions at the IVEM-TANDEM facility, Argonne National Laboratory. The results show that the T_c (critical temperature for amorphization) differs significantly between each series, e.g. for Y_2TiO_5 it is 589 ± 18 K and for $\text{Y}_2\text{Ti}_2\text{O}_7$ 665 ± 33 K. The difference suggests that recovery from damage is more rapid with increasing Ln content, i.e. a lower T_c for amorphization. These results are discussed in the context of the melting points of each phase, atomic disorder, the pyrochlore–fluorite order–disorder transition and the implications for oxide dispersion-strengthened additives.

© 2011 Acta Materialia Inc. Published by Elsevier Ltd. All rights reserved.

Keywords: Radiation damage; Pyrochlore; Oxide dispersion strengthened

1. Introduction

The resistance of materials to radiation damage is a vital factor when determining the ideal materials for use as a waste form [1], a new fuel type, e.g. inert matrix fuels (IMF), or other applications within the nuclear fuel cycle. However, it is not always possible to undertake experiments using radioactive decay as the time-scales can make the studies complex, difficult and expensive. One method for accelerating the effect of damage is ion beam irradiation [2], allowing systems to be studied rapidly and systematically. Two factors directly effecting radiation stability are the roles crystal structure and chemical composition play, i.e. which is the major component determining stability/recovery from damage [2–4]. As part of this process we have studied materials closely related to pyrochlore but which differ in composition, i.e. A_2BO_5 as opposed to $\text{A}_2\text{B}_2\text{O}_7$. In

this study we have prepared $\text{Y}_2\text{Ti}_2\text{O}_7$, Y_2TiO_5 , YbYTiO_5 , Yb_2TiO_5 and $\text{Yb}_2\text{Ti}_2\text{O}_7$ under identical conditions, subsequently irradiating them using the IVEM-TANDEM facility at Argonne National Laboratory.

The pyrochlore structure is well known, with many applications [5,6], examples of which include oxide fast ion conductors [7–12] and matrices for nuclear waste immobilization [2,13,14]. These applications are currently of major interest, as in both cases pyrochlores are capable of overcoming many technological problems while remaining cost effective. The ideal pyrochlore ($\text{A}_2\text{B}_2\text{O}_7$, $\text{A} = 2^+/3^+$, $\text{B} = 5^+/4^+$) structure can be described as a $2 \times 2 \times 2$ superstructure of fluorite (M_4X_8), with an ordered vacancy within the anion array. Such a vacancy allows the surrounding anions to relax from the ideal position in fluorite, giving rise to an observable superstructure in the anionic array. In conjunction with this relaxation the cations are ordered in chains, parallel to [110], with each cation species separated by $(\frac{1}{2}\frac{1}{2}\frac{1}{2})$, giving rise to an observable superstructure in the cation array. The addition of both superstructures changes the observed symmetry

* Corresponding author.

E-mail addresses: karlwhittle@me.com, karl.whittle@ansto.gov.au (K.R. Whittle).

from $Fm\bar{3}m$ to $Fd\bar{3}m$. This joint superstructure is visible using electron, X-ray or neutron diffraction and can be used to study the disordering processes within materials. An example structure is shown in Fig. 1a.

The general formulation $A_2B_2O_7$ is only one composition that can adopt the pyrochlore structure, with many containing vacancies [15] in A or B, e.g. AB_2O_6 . Previously it has been reported that Ln_2TiO_5 ($Ln_{2.67}Ti_{1.33}O_{6.67}$) can adopt the pyrochlore structure for the majority of lanthanides (Gd–Lu) [16,17]. For lanthanides below Gd an orthorhombic structure is adopted, with atypical Ti–O and Ln–O coordination [18]. However, between Gd and Ho the cubic phase is a high temperature phase, whereas between Er and Lu it is stable under ambient conditions. In this type of pyrochlore there is intrinsic disorder across one of the two cation sites, in this case the B site, and extra vacancies within the anionic array, i.e. Y_2TiO_5 is $Y_2(Ti_{1.33}Y_{0.67})O_{6.67}$ (shown in Fig. 1b). A further, but equally valid, application of $Y_2Ti_2O_7$ and Y_2TiO_5 (where the material is expected to adopt the orthorhombic structure) is as an additive within oxide dispersion strengthened (ODS) steels [19,20], however, how the oxide behaves under conditions commensurate with a nuclear core is still not fully understood. These structures provide a mechanism by which the effects of disorder in pyrochlores/fluorites can be examined as a function of radiation tolerance, with a minimal change in composition.

2. Experimental

Samples were prepared by the calcination of metal oxides using stoichiometric amounts of Y_2O_3 (Aldrich, 99.9%), Yb_2O_3 (Aldrich, 99.9%) and TiO_2 (99.9%) which had previously been heated at 850 °C for 12 h to remove any absorbed H_2O/CO_2 . The powders were ball milled to ensure complete mixing, pressed into pellets using cold isostatic pressing and heated at 1550 °C for 48 h, with heating and cooling rates of 5 K min^{-1} . Once cold the pellets were

crushed to a fine powder using a mortar and pestle and analysed using powder X-ray diffraction (XRD) to ensure the samples were single phase. The diffraction data were collected with a Panalytical X'pert Pro and an Xcellerator PSD in the range $2\theta = 5\text{--}80^\circ$, with an average step size of 0.01° and total count time of 100 s per point, with weighted $CuK\alpha$ radiation. The unit cell sizes were subsequently determined by Le Bail analysis [21] of the recorded patterns, using GSAS [22] and EXPGUI [23].

Selected area electron diffraction patterns were collected, prior to irradiation, using a JEOL 2010F transmission electron microscope, at an accelerating voltage of 200 keV. The samples were examined as crushed grains on holey carbon-coated Cu grids.

The samples were irradiated, again as crushed grains dispersed on a holey carbon-coated Cu grids, using the IVEM-TANDEM facility at the Argonne National Laboratory [24], with 1 MeV Kr^{2+} ions, in situ within a Hitachi 9000-NAR transmission electron microscope. A Gatan liquid helium (LHe) cooling stage was used for temperatures between 50 and 275 K, and a Gatan heating stage between room temperature and 650 K.

To minimize irradiation-induced temperature changes a fluence of 6.25×10^{11} ions $cm^{-2} s^{-1}$ was used, with the sample angled midway between the incident ion and electron beams, $\sim 15^\circ$ to the vertical. During irradiation the electron beam was switched off to prevent synergistic interactions of the electron and ion beams within the sample.

Multiple grains were irradiated simultaneously, with the point of amorphization being the point at which no Bragg diffraction intensities were visible in the selected area diffraction pattern. This is defined as the critical fluence (F_c) for the sample at the temperature of measurement. The data were subsequently analysed to determine the critical temperature (T_c), the temperature at which the rate of crystalline recovery is equal to the damage rate and above which the samples does not amorphize, under the same irradiation conditions. This temperature is determined by

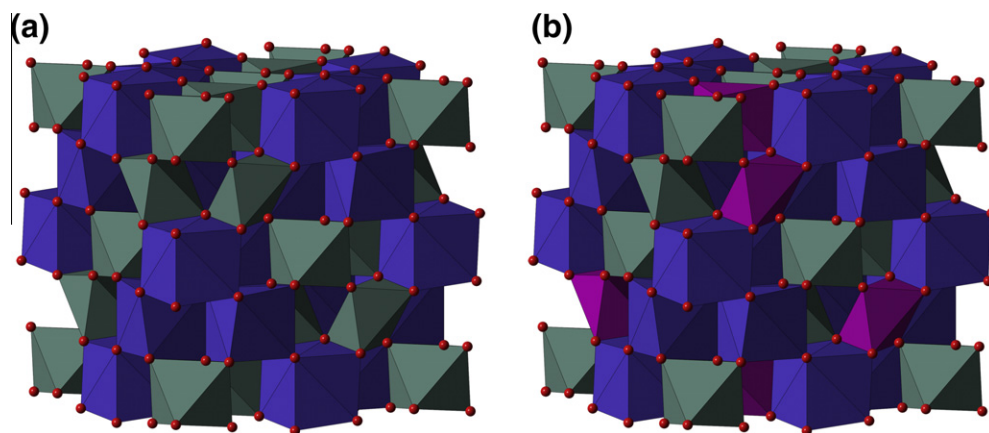


Fig. 1. Crystal structure representations of (a) $Ln_2Ti_2O_7$ and (b) $Ln_2Ti_{1.33}Ln_{0.67}O_{6.67}$ (Ln_2TiO_5). The changed colour in (b) is indicative of the replacement of Ti by Ln and does not represent the degree of ordering. (For interpretation of the references to colour in this figure legend, the reader is referred to the web version of this article.)

least squares numerical analysis of critical fluence against temperature. The equation used for this process [25] is shown below (Eq. (1)), and is used to determine T_c and the critical fluence at 0 K (F_{c0}), which is inversely proportional to the damage cross-section for the system under analysis, and the energy of activation for crystalline recovery (E_a), using the Boltzmann constant ($k_b = 8.617342 \times 10^{-5} \text{ eV K}^{-1}$):

$$F_c = \frac{F_{c0}}{1 - \exp\left[\frac{E_a/k_b}{T_c} \left(\frac{1}{T_c} - \frac{1}{T}\right)\right]} \quad (1)$$

It has been reported in the literature that the energy of activation for recovery is often underestimated using this approach, and an approach based on other non-kinetic factors has been suggested by Weber [26]:

$$E_a = T_c \left[k_b \ln \left(\frac{F_{c0} \nu}{\phi} \right) \right] \quad (2)$$

This approach uses the critical fluence at 0 K (F_{c0}), incident ion flux $\phi = 6.25 \times 10^{11} \text{ ions cm}^{-2} \text{ s}^{-1}$ and the effective jump frequency ν , assumed to be 10^{12} . Values for T_c and F_{c0} can be estimated from the recorded data or the values obtained from Eq. (1) can be used.

3. Results and discussion

The recorded XRD patterns for all samples are shown in Fig. 2. All samples were found to be single phase, and by XRD were ordered pyrochlore ($\text{Y}_2\text{Ti}_2\text{O}_7$, $\text{Yb}_2\text{Ti}_2\text{O}_7$ and Y_2TiO_5), or disordered fluorite (YbYTiO_5 and Yb_2TiO_5). The lattice parameters determined by a Le Bail analysis of the recorded patterns using GSAS/EXPGUI, are shown in Table 1, along with the calculated Ra/Rb ratios. The

Table 1
Refined lattice parameters using the Le Bail method.

System	Lattice parameter (Å)	Ra/Rb
$\text{Y}_2\text{Ti}_2\text{O}_7$	10.0577 (1)	1.68
$\text{Yb}_2\text{Ti}_2\text{O}_7$	10.0356 (7)	1.63
Y_2TiO_5	10.2558 (11)	1.45
YbYTiO_5	5.1008 (5)	1.44
Yb_2TiO_5	5.0744 (5)	1.42

The ESD (shown in parentheses) are those calculated using GSAS. The lattice parameters for YbYTiO_5 and Yb_2TiO_5 are based on the fluorite unit cell, $a/2$ compared with pyrochlore, whereas the others are based on the pyrochlore unit cell.

Ra/Rb ratios are based on Shannon's radii, and based on $\text{Ln}_2\text{Ti}_{1.33}\text{Ln}_{0.67}\text{O}_{6.67}$ formulations, while the YbYTiO_5 calculation assumes 1:1 occupancy of the A and B sites by Yb and Y.

Electron diffraction was additionally used to confirm the existence of superstructure, i.e. pyrochlore and not fluorite (no superstructure) formation. During the analysis it became apparent that not only did the $\text{Ln}_2\text{Ti}_2\text{O}_7$ systems adopt a pyrochlore form with the expected $2 \times 2 \times 2$ superstructure, but that the Ln_2TiO_5 systems showed evidence of ordering equivalent to pyrochlore. This ordering is long-range (domains/volumes sufficient for scattering) with regard to transmission electron microscopy (TEM) but short-range with regard to XRD (lack of large domains) giving rise to an XRD pattern equivalent to fluorite, i.e. showing no evidence of superstructure. In Y_2TiO_5 , which showed pyrochlore superstructure peaks in XRD, there were further spots visible, indicating a possible tripling of the pyrochlore unit cell in the 111 direction, visible along the [110] zone axis, shown in Fig. 3. This ordering is not fully understood, but has also been seen in Ho_2TiO_5 by

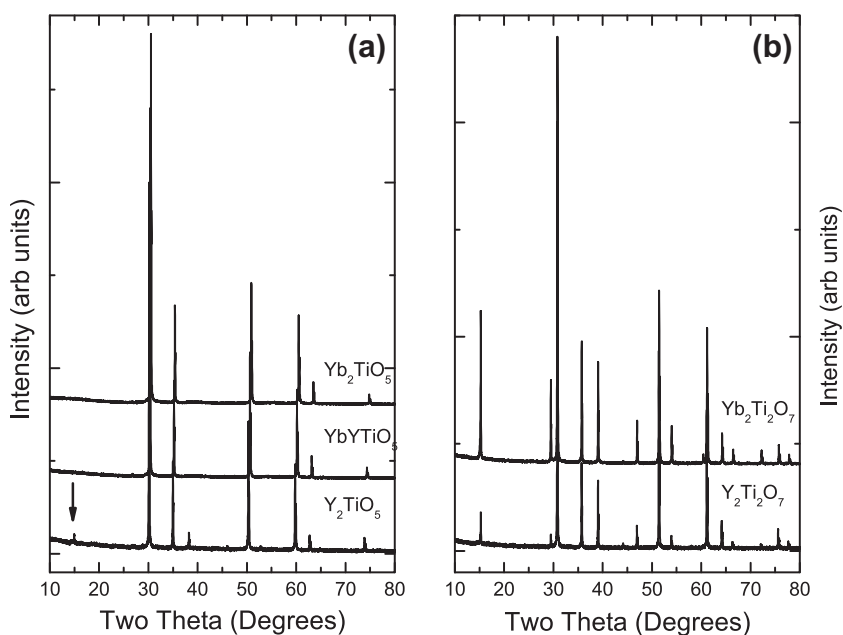


Fig. 2. X-ray diffraction patterns showing the single-phase nature of the samples being studied. In (a) the arrow highlights the position for which the pyrochlore superstructure is visible for Y_2TiO_5 , but is not visible in either YbYTiO_5 or Yb_2TiO_5 for the samples irradiated.

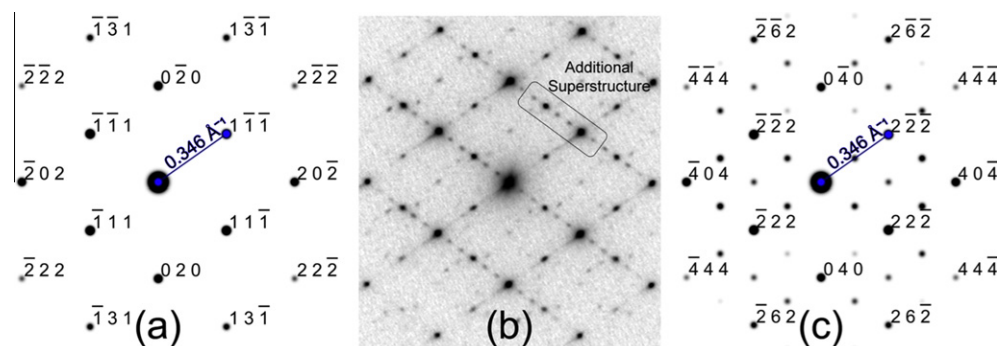


Fig. 3. (a) Simulated kinematic electron diffraction pattern for the $\langle 101 \rangle$ zone axis of fluorite, (b) selected-area diffraction from $Y_2Ti_2O_7$, down the $\langle 101 \rangle$ zone axis, showing evidence for superstructure along the $[111]$ direction, and (c) simulated kinematic electron diffraction pattern for the $\langle 101 \rangle$ zone axis in the pyrochlore. The distance shown is the equivalent reciprocal space length for similar spots, showing the double nature of the pyrochlore lattice parameter. (b) has been modified to highlight the weak nature of the superstructure intensities.

Lau et al. [16,17,27], and is the subject of further work using high resolution electron imaging, coupled with further diffraction studies. There was additional evidence for the second degree of ordering found by Lau et al. [16,17,27] along the 662 direction, although these spots were difficult to observe.

As outlined above, the samples were irradiated at a variety of temperatures, and at each temperature the F_c was determined, with an error based on the fluence steps and spread of data. F_{c0} , T_c and E_a are shown, along with the ratio of electronic to nuclear stopping power (ENSP), calculated using SRIM2008 [28,29], in Table 2 and are plotted in Fig. 4. The results obtained here for $Y_2Ti_2O_7$ and $Yb_2Ti_2O_7$ are both lower than those previously reported by Lian et al. [30]. This difference is most likely due to the different methods of sample preparation, i.e. single crystal growth vs. solid state sintering, coupled with slight differences in the irradiation conditions. However, the trend is in agreement, i.e. there is a decrease in T_c from Y to Yb. The calculated ENSP suggest that in these samples the main method for retarding incident ions is through nuclear interaction ($ENSP < 1$), i.e. impact, with less energy being transferred through electronic excitation and transfer. Therefore, a structural cause for the change in T_c cannot and should not be discounted, and should be included in any discussion. However, since these structures are broadly similar the differences due to structure are expected to be small, with a bigger change arising from the formation and effects of disorder.

Using the methodologies previously suggested by Naguib and Kelly [31] relating the melting point for a system to the T_c for amorphization, and similar observations made by Lam et al. [32,33] correlating static disorder with the melting point, the trend in T_c can be related to both the melting point and static disorder, i.e. cation mixing at the B site. The melting point for Y_2O_3 is 2633 K, while for Yb_2O_3 it is 2708 K (Table 3), with being highly tolerant of damage, with a T_c of less than 50 K under similar conditions. A close relation of this system Dy_2O_3 has previously been studied by Tang et al. [34] and found to undergo a crystalline transition from cubic to monoclinic. Since Dy_2O_3 adopts the same bixbyite structure as Y_2O_3 and Yb_2O_3 , the same transformation is expected here. In these samples it is difficult to extract direct relationships with the melting point as the melting points of $Y_2Ti_2O_7$, Y_2TiO_5 and $YbYTiO_5$ have not been determined experimentally. The melting point of TiO_2 is 2123 K, and has previously been studied under similar conditions of irradiation and shown to have a range of different T_c for amorphization dependent on the polymorph being studied, with anatase having the highest T_c of 242(6) K. This system has been further discussed in Lumpkin et al. [4,35].

The crystal structures for all the systems studied are relatable to fluorite. Pyrochlore is classically a $2 \times 2 \times 2$ superstructure of fluorite with cation ordering and an ordered $1/8$ vacancy in the anion array for charge compensation. Bixbyite (Y_2O_3) is similar to fluorite in terms of cation location, i.e. broadly a face centred array, but with a

Table 2
Fitted results from analysis of damage data, and the calculated electronic to nuclear stopping power (ENSP) using SRIM2008.

System	T_c (K)	F_{c0} ($\times 10^{14}$ ions cm^{-2})	E_a (eV)		ENSP
			Eq. (1)	Eq. (2)	
$Y_2Ti_2O_7$	665 (33)	4.75 (0.5)	0.6 (1.06)	1.96 (0.1)	0.742
$Yb_2Ti_2O_7$	594 (22)	6.57 (0.8)	0.24 (0.11)	1.77 (0.07)	0.681
Y_2TiO_5	589 (17)	4.02 (0.42)	0.07 (0.01)	1.73 (0.06)	0.727
$YbYTiO_5$	467 (2)	5.07 (0.09)	0.43 (0.04)	1.38 (0.01)	0.688
Yb_2TiO_5	457 (27)	3.60 (0.6)	0.08 (0.04)	1.34 (0.09)	0.652

The atomic displacement energies used in SRIM2008 are 50 eV for each species.

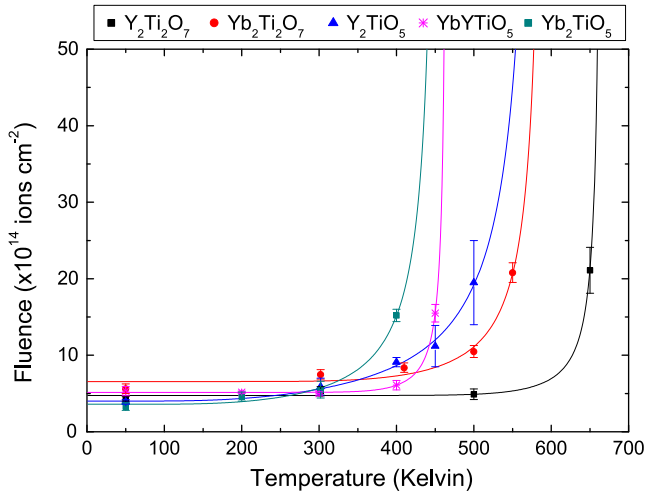


Fig. 4. Plots of critical fluence (F_c) as a function of temperature. The curves are fitted using Eq. (1). The values obtained from the curve fitting are shown in Table 1.

Table 3
The T_c values obtained and previously published melting points.

System	T_c (K)	Melting point (K)	References
$Y_2Ti_2O_7$	665 (33)	~2160	[53,54]
$Yb_2Ti_2O_7$	594 (22)	2163	[40]
	589 (17)	~2120	[53,54]
$YbYTiO_5$	467 (2)		
Yb_2TiO_5	457 (27)	2353	[55]

The values for $Y_2Ti_2O_7$ and Y_2TiO_5 are estimates from Schaedler et al. [53,54]. There is no reported data for $YbYTiO_5$.

modified anion array. In fluorite every cation tetrahedral interstice is occupied (in pyrochlore this is modified by removal of 1/8), while in bixbyite 3/4 are occupied (maintaining charge balance). Classically bixbyite is defined as body centred, adopting $Ia\bar{3}d$ symmetry, while fluorites are face centred structures adopting an $Fm\bar{3}m$ structure. However, they can all be described as fluorites, all essentially being different disordered/ordered forms.

As has previously been noted in the literature, $Y_2Ti_2O_7$ is highly ordered with minimal disorder across the A(Y) and B(Ti) sites [36–38]. A similar observation is expected for $Yb_2Ti_2O_7$, and indeed simulations by Jiang et al. using density functional theory (DFT)-based techniques [39] have suggested that disordering of both $Y_2Ti_2O_7$ and $Yb_2Ti_2O_7$ is energetically unfavourable up to the melting point, and thus unlikely to occur. Shlyakhtina et al. [40,41] observed ~5% mixing between Yb and Ti on the A and B sites, using data from Rietveld refinement of XRD data recorded for $Yb_2Ti_2O_7$ heated under similar conditions, however, the exact heating regime was not stated. Hence, for the purposes of this discussion these phases are considered ordered with minimal (zero) cation anti-site disorder.

When Y_2TiO_5/Yb_2TiO_5 are compared with $Y_2Ti_2O_7/Yb_2Ti_2O_7$ the cationic disorder immediately increases. By

their nature both of these systems have cation mixing on the B site. When normalized the composition of, for example, Y_2TiO_5 becomes $Y_2[Ti_{1.33}Y_{0.67}]O_{6.67}$, with a B site fractional occupancy of 2/3 Ti and 1/3 Y. Such mixing can be ordered with the formation of a large supercell, as seen by Lau et al. [16,17,27] for Ho_2TiO_5 and here for Y_2TiO_5 in the recorded XRD patterns and TEM images. They can also form with cation disorder as a fluorite with no observable superstructure, as previously reported by Shlyakhtina et al. [9–11] for Yb_2TiO_5 . Previously Lau et al. [16,17,27] reported that Yb_2TiO_5 can be ordered similarly to pyrochlore, however, the neutron diffraction patterns showed a broad diffuse peak where the 331 peak would be located. Electron diffraction patterns, shown in Fig. 5, suggest that both Yb_2TiO_5 and $YbYTiO_5$ adopt the pyrochlore form on the nanoscale with small nanoscale domains (shown by dark field imaging), similar to that found by Lau et al. [16,17,27]. A major difference between these phases and Y_2TiO_5 is that the superstructure spots expected from pyrochlore-type ordering are more diffuse in Yb_2TiO_5 and $YbYTiO_5$ than in Y_2TiO_5 , indicating an ordering with some variability in distance, i.e. not exactly $2 \times 2 \times 2$ fluorite. However ordered, they are still more disordered than their fully ordered pyrochlore equivalents, due to the ordering being visible only with electron diffraction, and hence they form nano-domains.

If this methodology for describing disorder is applied to Y_2O_3/Yb_2O_3 a contrasting kind of order/disorder is found. As outlined above, bixbyite is related to fluorite and can be thought of as fluorite with positional displacements for both cations and anions. For example the Y^{3+}/Yb^{3+} array is essentially fluorite, i.e. a fcc arrangement, with the O^{2-} anions located in tetrahedral holes. Both arrays then move away from the ideal positions expected in fluorite, minimizing the lattice energy of the system. Bixbyite is thus related to pyrochlore, but only in the “ideal” case, i.e. they are both fcc arrangements of cations with anions filling tetrahedral holes. However, when both types of disorder are compared some comparisons can be made.

In these samples pyrochlore is the most ordered, i.e. the base, adopted by $Y_2Ti_2O_7$ and $Yb_2Ti_2O_7$, where disorder is either not preferred or observed in these samples. Thus Y_2TiO_5 would be the first disordered system, with ordering on the longer scale, i.e. visible in XRD measurements (Fig. 2) indicating ordering on a length scale for coherent diffraction. However, since both Y^{3+} and Ti^{4+} exist at the B site, for the purposes of this discussion it is disordered, i.e. Y^{3+} is found on both the A and B sites. The most disordered systems in this study are Yb_2TiO_5 and $YbYTiO_5$, which have been shown by XRD to be defect fluorite and therefore on the longer scale are disordered, while on the nanoscale they were found by TEM to be ordered. Therefore, with increasing disorder the sequence of ordered samples is $Y_2Ti_2O_7/Yb_2Ti_2O_7$, Y_2TiO_5 , Yb_2TiO_5 and $YbYTiO_5$. Technically the $YbYTiO_5$ system has more disorder than Yb_2TiO_5 due to three cations present in the system, however, in reality they are likely to be almost identical

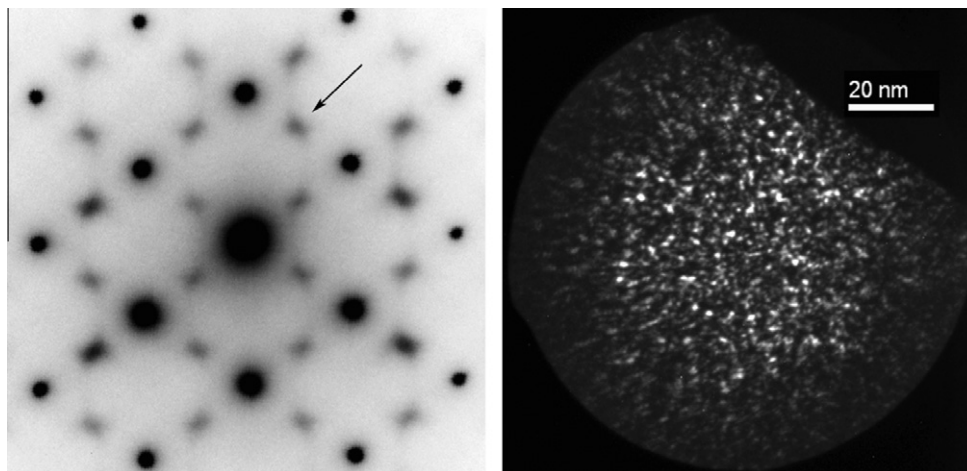


Fig. 5. A selected-area diffraction pattern from Yb_2TiO_5 , along the $\langle 101 \rangle$ zone axis with the corresponding dark-field image, showing the diffuse nature of the peaks associated with ordering within the lattice, and the small size, of the order of nanometers, of the domains. The dark-field image was recorded using a broad diffuse peak, such as the one highlighted. The streaking is along the $[111]$ direction, indicating a degree of ordering along this direction.

in terms of disorder as they both form defect fluorite arrays with only short-range ordering.

Finally, as outliers that are contrastable but not directly comparable, there are $\text{Y}_2\text{O}_3/\text{Yb}_2\text{O}_3$, which are disordered but in a positional manner whereby the lattice is stabilized by moving the component atoms off symmetrically ideal sites. This can be considered to have the highest positional disorder in cation location, but with a high degree of order as the cation is monotonic, i.e. Y^{3+} or Yb^{3+} , whereas the others have at least two cations. Thus, as these have proven to remain crystalline at temperatures above 50 K (the lowest temperature measured here), they are assumed to be highly tolerant of damage, but can transform from bixbyite (C-type rare earth oxide) to a monoclinic B-type rare earth oxide at higher levels of damage [34,42,43].

If this methodology for determining order and disorder is compared with the observed T_c values, the more disordered a system is the lower the T_c . As can be seen both YbYTiO_5 and Yb_2TiO_5 have similar values for T_c , but as outlined above they also have similar levels of disorder. The radiation responses of $\text{Y}_2\text{O}_3/\text{Yb}_2\text{O}_3$ agree with increased static disorder in the structure, but as it is positional disorder it is difficult to compare directly.

Once a damage cascade begins and atoms become displaced from their original positions how the material behaves depends on its ability to recover from damage. If the material, for example $\text{Y}_2\text{Ti}_2\text{O}_7$, shows no evidence of cation disorder then recovery to a stable disordered system is unlikely, however, formation of a metastable phase is possible, but is itself thermodynamically unstable and therefore should transform to a more stable state with either increasing temperature or irradiation. However, if the system can accommodate static disorder, e.g. YbYTiO_5 , then recovery to a stable lower lattice energy state can occur more easily, giving rise to a lower T_c . This hypothesis agrees with those proposed by Lam et al. [32,33], who linked static disorder to the ability of a system

to recover from damage. In these systems the ability to tolerate static disorder directly affects the radiation response.

A similar response was previously reported [18] for the systems $\text{La}_2\text{Ti}_2\text{O}_7$, $\text{La}_{2/3}\text{TiO}_3$ and La_2TiO_5 , with $\text{La}_2\text{Ti}_2\text{O}_7$ and $\text{La}_{2/3}\text{TiO}_3$ having significantly lower T_c values for amorphization, under identical irradiation conditions, than La_2TiO_5 . The major difference between these phases is that La_2TiO_5 is a highly ordered structure with atypical coordination of both La and Ti (7 and 5, respectively). It is expected that the cation anti-site energies for La_2TiO_5 would be high due to atypical coordination of Ti^{4+} , a square based pyramid, preventing stable occupancy by La^{3+} . In contrast, both $\text{La}_2\text{Ti}_2\text{O}_7$ and $\text{La}_{2/3}\text{TiO}_3$ have high levels of positional ($\text{La}_2\text{Ti}_2\text{O}_7$) and occupancy ($\text{La}_{2/3}\text{TiO}_3$) disorder. These types of disorder give rise to many more stable intermediate arrangements during recovery from damage.

Such linkage with stable static disorder has been observed in other fluorite-based systems, with those that can tolerate disorder tending to have lower observed T_c values than those which do not. Examples [2,44] of this are $\text{La}_2\text{Hf}_2\text{O}_7$ and $\text{La}_{1.6}\text{Y}_{0.4}\text{Hf}_2\text{O}_7$, where $\text{La}_2\text{Hf}_2\text{O}_7$ is a fully ordered pyrochlore with La^{3+} at the A site and Hf^{4+} at the B site. However, $\text{La}_{1.6}\text{Y}_{0.4}\text{Hf}_2\text{O}_7$ is more disordered with Hf^{4+} at the B site, but the A site now contains La^{3+} and Y^{3+} , with no further ordering observed [45]. The T_c for $\text{La}_2\text{Hf}_2\text{O}_7$ is 563(22) K and for $\text{La}_{1.6}\text{Y}_{0.4}\text{Hf}_2\text{O}_7$ is 473(52) K, a small but significant change in agreement with the discussion above. However, the system $\text{Y}_2\text{Sn}_{2-x}\text{Ti}_x\text{O}_7$ does not. In this system the T_c changes from 665(33) for $\text{Y}_2\text{Ti}_2\text{O}_7$ to remaining crystalline at 50 K for both $\text{Y}_2\text{Sn}_{1.6}\text{Ti}_{0.4}\text{O}_7$ and $\text{Y}_2\text{Sn}_2\text{O}_7$ under the conditions of irradiation, i.e. 1 MeV Kr. If these systems followed the disorder approach the minimum T_c would be for Y_2SnTiO_7 , i.e. a 1:1 mix at the B site with maximum disorder, with T_c increasing on either side as ordering increases. However, this is not found, and T_c decreases across the series until

the samples remain crystalline under these irradiation conditions at 50 K. The increase in stability from $\text{Y}_2\text{Ti}_2\text{O}_7$ to $\text{Y}_2\text{Sn}_2\text{O}_7$ under these conditions of irradiation is complex but can be correlated with disorder. Previously [36–38] it has been found that there is no A and B site mixing within the $\text{Y}_2\text{Sn}_{2-x}\text{Ti}_x\text{O}_7$ system. There is random disorder across the B site, i.e. Sn/Ti is random and not ordered, but this is restricted to the B site. This type of disorder is different to that in the samples studied here, but they share some similarities, for example as the Sn content increases the T_c decreases, i.e. increased disorder is accompanied by increasing stability. However, if static/chemical disorder alone was determining stability the T_c would continue to decrease at Y_2SnTiO_7 , where the system should have the lowest T_c . At this point the effects of Sn and the increased stability within the pyrochlore lattice become apparent. The increasing stability drives the recrystallization process to form a pyrochlore/fluorite. Previous work by Ewing et al. [46] suggested that $\text{Y}_2\text{Sn}_2\text{O}_7$ becomes disordered under irradiation to form a defect fluorite, however, we believe that the sample remains a pyrochlore but that the pyrochlore superlattice points in the electron diffraction pattern become weaker due to the loss of long-range order, as the material forms nanodomains. The loss of superlattice points is similar to the lack of superlattice reflections seen in the XRD patterns for Yb_2TiO_5 (Fig. 2) [47].

Increased stability of $\text{Ln}_2\text{Sn}_2\text{O}_7$ pyrochlores is well known and has been used to explain the formation of ordered pyrochlores when classical methods to determine pyrochlore stability suggest they should form a defect fluorite, i.e. $R_a/R_b = 1.48\text{--}1.78$. If the radius ratio alone defined the $\text{Ln}_2\text{Sn}_2\text{O}_7$ pyrochlore stability range then La–Dy would form a pyrochlore structure, with Ho–Lu forming a fluorite structure, similarly to the $\text{Ln}_2\text{Zr}_2\text{O}_7$ system. However, Kennedy et al. [48] have shown that $\text{Lu}_2\text{Sn}_2\text{O}_7$ is a pyrochlore, suggesting that some other factor is driving the formation of pyrochlore. In these systems the Sn–O interaction is strong, driving the formation of pyrochlore when other factors, such as ionic radius stability calculations, indicate it should be fluorite [49]. Thus in these samples the effect of increased disorder decreasing the T_c is offset by internal bonding driving reformation of the pyrochlore structure. In the samples studied here the Ti–O interaction is less strong than the Sn–O interaction within pyrochlore structures, thus removing a secondary factor determining stability.

A secondary factor that cannot be discounted for the increase in radiation tolerance/rapid recovery is the vacancies and increased static disorder at the anionic sites. As the formulation of the Ln_2TiO_5 phases is $\text{Ln}_2\text{Ti}_{1.33}\text{Ln}_{0.67}\text{O}_{6.67}$ there are implicit vacancies within the anion array compared with $\text{Ln}_2\text{Ti}_2\text{O}_7$. Such vacancies should increase the conductivity of these phases with respect to the $\text{Ln}_2\text{Ti}_2\text{O}_7$ phases. Previous work by Pirzada et al. [50] proposed a mechanism for oxygen conductivity in pyrochlore systems utilizing vacancy hopping between the 48f positions via unoccupied lattice positions. Such a mechanism would

be enhanced in these systems by the extra vacancies required for charge compensation. Previous work by Shlyakhtina et al. [9,11,12,51,52] and Yamamura et al. [7,8] has shown that an increase in disorder increases the anionic conductivity. However, a change from pyrochlore to fluorite, as found by Yamamura et al. [7,8] significantly reduces the conductivity, implying that large-scale disorder, e.g. complete site mixing, is detrimental to anionic conductivity. Therefore, these systems, with their partial disorder across the B site, would have increased anionic conductivity, which would aid recovery of the lattice from damage.

The results show that the formation/use of cubic Y_2TiO_5 as opposed to fully ordered $\text{Y}_2\text{Ti}_2\text{O}_7$ could greatly enhance the resistance to, or recovery from, radiation damage within ODS materials. One interesting thing to note is that cubic Yb_2TiO_5 is seemingly more resistant to damage than cubic Y_2TiO_5 , which may be an advantage when designing new materials for use in extreme radiation fields, e.g. GenIV fission systems.

4. Conclusion

Stuffed pyrochlores (Ln_2TiO_5) are more resistant to damage than classical pyrochlores ($\text{Ln}_2\text{Ti}_2\text{O}_7$). The T_c is significantly reduced with B site disorder, implying that disorder, whether positional or chemical, significantly reduces the T_c for recrystallization. However, the effect is weak compared with other factors that define structure—for example a strong preference for ordering helps stabilize the structure. This effect is being further investigated using DFT and molecular dynamics simulations in concert with these results to elucidate possible mechanisms for recovery, and whether there is a systematic cause of structural recovery which is present but not easily visible in these systems.

Acknowledgements

We wish to acknowledge the help of the staff at the Electron Microscopy Center, in particular Peter Baldo, Edward Ryan, and Marques Kirk, for their efficient and continued running of the IVEM-TANDEM facility. The IVEM-TANDEM facility is supported as a User Facility by the US Department of Energy, Basic Energy Sciences, under Contract W-31-10-ENG-38. We acknowledge the funding provided by the Access to Major Facilities Research Programme (a component of the International Science Linkages programme established under the Australian government's innovation statement, Backing Australia's Ability).

References

- [1] Ewing RC, Weber WJ, Clinard F. Prog Nucl Energy 1995;29:63.
- [2] Lumpkin GR, Smith KL, Blackford M, Whittle KR, Harvey EJ, Redfern SAT, et al. Chem Mater 2009;21:2746.
- [3] Lumpkin GR, Pruneda M, Rios S, Smith KL, Trachenko K, Whittle KR, et al. J Solid State Chem 2007;180:1512.
- [4] Lumpkin GR, Smith KL, Blackford M, Thomas BS, Whittle KR. Phys Rev B 2008;77:214201.

- [5] Subramanian MA, Aravamudan G, Subba Rao GV. *Prog Solid State Chem* 1983;15:55.
- [6] Chakoumakos B. *J Solid State Chem* 1984;53:120.
- [7] Yamamura H, Nishino H, Kakinuma K, Nomura K. *J Ceram Soc Jpn* 2003;111:902.
- [8] Yamamura H, Nishino H, Kakinuma K, Nomura K. *Solid State Ion* 2003;158:359.
- [9] Abrantes JCC, Levchenko A, Shlyakhtina AV, Shcherbakova LG, Horovistiz AL, Fagg DP, et al. *Solid State Ion* 2006;177:1785.
- [10] Levchenko A, Abrantes J, Shlyakhtina A, Shcherbakova L, Horovistiz A, Frade J. *Mater Sci Forum* 2006;514–516:417.
- [11] Shlyakhtina AV, Savvin SN, Levchenko AV, Boguslavskii MV, Shcherbakova LG. *Solid State Ion* 2008;179:985.
- [12] Shlyakhtina A, Abrantes J, Levchenko A, Stefanovich S, Knot'ko A, Larina L, et al. *Mater Sci Forum* 2006;514–516:422.
- [13] Ewing R, Weber W, Lian J. *J Appl Phys* 2004;95:5949.
- [14] Ewing RC. *Prog Nucl Energy* 2007;49:635.
- [15] Whittle KR, Lumpkin GR, Ashbrook S. *J Solid State Chem* 2006;179:512.
- [16] Lau GC, McQueen TM, Huang Q, Zandbergen HW, Cava RJ. *J Solid State Chem* 2008;181:45.
- [17] Lau G, Muegge BD, McQueen T, Duncan E, Cava R. *J Solid State Chem* 2006;179:3126.
- [18] Whittle KR, Lumpkin GR, Blackford M, Aughterson RD, Smith KL, Zaluzec NJ. *J Solid State Chem* 2010;183:2416.
- [19] Jiang Y, Smith J, Robert Odette G. *Acta Mater* 2010;58:1536.
- [20] Odette G, Alinger M, Wirth B. *Annu Rev Mater Res* 2008;38:471.
- [21] Le Bail A, Duroy H, Fourquet J. *Mater Res Bull* 1988;23:447.
- [22] Larson A, Von Dreele R. Los Alamos National Laboratory report LAUR 86-748. Los Alamos (NM): Los Alamos National Laboratory; 1994. p. 86.
- [23] Toby B. *J Appl Crystallogr* 2001;34:210.
- [24] Allen C, Funk LR, Ryan EA. *Mater Res Soc Symp Proc* 1996;396:641.
- [25] Wang SX, Wang L, Ewing RC. *Mater Res Soc Symp Proc* 1997;504:165.
- [26] Weber WJ. *Nucl Instrum Methods Phys Res Sect B Beam Interact Mater Atoms* 2000;166/167:98.
- [27] Lau GC, Freitas RS, Ueland BG, Dahlberg ML, Huang Q, Zandbergen HW, et al. *Phys Rev B* 2007;76:054430.
- [28] Ziegler J. *Nucl Instrum Methods Phys Res Sect B Beam Interact Mater Atoms* 2004;219:1027.
- [29] Ziegler J, Ziegler M, Biersack J. *Nucl Instrum Methods Phys Res Sect B Beam Interact Mater Atoms* 2010;268:1818.
- [30] Lian J, Wang L, Chen J, Sun K, Ewing RC, Matt Farmer J, et al. *Acta Mater* 2003;51:1493.
- [31] Naguib H, Kelly R. *Radiat Effects Defects Solids* 1975;25:1.
- [32] Lam NQ, Okamoto PR. *Surf Coat Technol* 1994;65:7.
- [33] Lam N, Okamoto P, Li M. *J Nucl Mater* 1997;251:89.
- [34] Tang M, Valdez J, Sickafus K, Lu P. *Appl Phys Lett* 2007;90:151907.
- [35] Lumpkin GR, Blackford M, Smith KL, Whittle KR, Zaluzec NJ, Ryan EA, et al. *Am Mineral* 2010;95:192.
- [36] Mitchell MR, Reader SW, Johnston KE, Pickard CJ, Whittle KR, Ashbrook SE. *Phys Chem Chem Phys* 2011;13:488.
- [37] Reader SW, Mitchell MR, Johnston KE, Pickard CJ, Whittle KR, Ashbrook SE. *J Phys Chem C* 2009;113:18874.
- [38] Ashbrook S, Whittle KR, Lumpkin GR, Farnan I. *J Phys Chem B* 2006;110:10358.
- [39] Jiang C, Stanek CR, Sickafus KE, Uberuaga BP. *Phys Rev B* 2009;79:104203.
- [40] Shlyakhtina A, Abrantes J, Larina L, Shcherbakova L. *Solid State Ion* 2005;176:1653.
- [41] Shlyakhtina A, Shcherbakova L, Knotko A, Steblevskii A. *J Solid State Electr* 2004;8:661.
- [42] Tang M, Valdez JA, Sickafus KE, Lu P. *Jom-Us* 2007;59:36.
- [43] Kittiratanawasin L, Smith R, Uberuaga BP, Sickafus KE. *J Phys Condens Matter* 2009;21:115403.
- [44] Lumpkin GR, Whittle KR, Rios S, Smith KL, Zaluzec N. *J Phys Condens Matter* 2004;16:8557.
- [45] Whittle KR, Cranswick LMD, Redfern SAT, Swainson IP, Lumpkin GR. *J Solid State Chem* 2009;182:442.
- [46] Ewing RC, Lian J, Wang L. *Mater Res Soc Symp Proc* 2004;792:R2.1.1.
- [47] Lumpkin GR, Blackford M, Smith KL, Whittle KR, Zaluzec N. *Microsc Microanal* 2009;15(Suppl. 2):1358.
- [48] Kennedy B, Hunter B, Howard C. *J Solid State Chem* 1997;130:58.
- [49] Srivastava AM, Brik MG. *J Lumin* 2010;1.
- [50] Pirzada M, Grimes R, Minervini L, Maguire J, Sickafus K. *Solid State Ion* 2001;140:201.
- [51] Shlyakhtina A, Kolbanov I, Knotko A, Boguslavskii M, Stefanovich S, Karyagina O, et al. *Inorg Mater* 2005;41:854.
- [52] Shlyakhtina A, Mosunov A, Stefanovich S, Karyagina O, Shcherbakova L. *Inorg Mater* 2004;40:1317.
- [53] Schaedler T, Fabrichnaya O, Levi C. *J Eur Ceram Soc* 2008;28:2509.
- [54] Schaedler T, Francillon W, Gandhi A, Grey C, Sampath S, Levi C. *Acta Mater* 2005;53:2957.
- [55] Shamrai G, Zagorodnyuk A, Magunov R. *Inorg Mater* 1992;28:1633.